Complex embryos displaying bilaterian characters from Precambrian Doushantuo phosphate deposits, Weng'an, Guizhou, China

Jun-Yuan Chen[a,1], David J. Bottjer[b], Gang Li[c], Michael G. Hadfield[d], Feng Gao[e], Andrew R. Cameron[e], Chen-Yu Zhang[a], Ding-Chang Xian[c], Paul Tafforeau[f], Xin Liao[a], and Zong-Jun Yin[a]

[a]LPS of Nanjing Institute of Geology and Paleontology, Institute of Evo/Developmental Biology, and State Key Laboratory of Pharmaceutical Biotechnology, Nanjing University, Nanjing 210093, China; [b]Department of Earth Sciences, University of Southern California, Los Angeles, CA 90089; [c]Institute of High Energy Physics, Beijing 100049, China; [d]Kewalo Marine Laboratory, University of Hawaii at Manoa, Honolulu, HI 96813; [e]Division of Biology, 156-29, California Institute of Technology, Pasadena, CA 91125; and [f]European Synchrotron Radiation Facility, F-38043 Grenoble, France

Edited by J. William Schopf, University of California, Los Angeles, CA, and approved September 18, 2009 (received for review May 5, 2009)

Three-dimensionally preserved embryos from the Precambrian Ediacaran Doushantuo Formation, Weng'an, Guizhou, southern China, have attracted great attention as the oldest fossil evidence yet found for multicellular animal life on Earth. Many embryos are early cleavage embryos and most of them yield a limited phylogenetic signal. Here we report the discovery of two Doushantuo embryos that are three-dimensionally preserved and complex. Imaging techniques using propagation phase-contrast based synchrotron radiation microtomography (PPC-SR-μCT) reveal that the organization of cells demonstrates several bilaterian features, including the formation of anterior-posterior, dorso-ventral, and right-left polarities, and cell differentiation. Unexpectedly, our observations show a noticeable difference in organization patterns between the embryos, suggesting that they represent two distinct taxa. These embryos provide further evidence for the presence of bilaterian animals in the Doushantuo biota. Furthermore, these bilaterians had already diverged into distantly related groups at least 40 million years before the Cambrian radiation, indicating that the last common ancestor of the bilaterians lived much earlier than is usually thought.

early animal evolution | early metazoan evolution | nondestructive 3-D reconstruction | precambrian ediacaran embryos | Weng'an biota

Many fossil embryos are known from the Weng'an Phosphate Member of the Ediacaran Doushantuo Formation (580–600 Ma) (1–3). Among these, embryos at an advanced stage of development with complex organization are uncommon (4–11). Although some are advanced with up to 2,600 cells, these advanced stage embryos remain simple, exhibiting no evidence of patterning organization, or even cell differentiation (4) (Fig. S1). Traditional methods for the study of Doushantuo embryos are by petrologic thin section, or alternatively, by examination of external form with scanning electron microscopy (SEM). But reconstruction of the whole form is difficult by the first of these methods, while examination of internal structure is impossible by the second. Propagation phase contrast-based synchrotron radiation microtomography (PPC-SR-μCT) is an effective way to address both these problems (6, 11–15). It is not only nondestructive, but also can reveal many structures that are invisible, or hardly visible, by the classical absorption contrast-based imaging technique. Here we describe a digital analysis of PPC-SR-μCT data obtained at the European Synchrotron Radiation Facility ID19 beamline from two fossil embryos from the Doushantuo Formation.

Results

Among the approximately 100 embryos that we have studied using PPC-SR-μCT, two are remarkable, displaying a complex organization similar to that found in modern bilaterian embryos. The first of these specimens (4F10) is an embryo at the 32-cell stage with some cells missing. The cell number was determined by counting all cells visible in tomographic sections and noting broken areas on the surface of the embryo that appear to be the remnants of missing blastomeres (Movie S1). Through examination of various external views and internal sections an understanding can be gained of polarity and cell differentiation in this embryo (Figs. 1 and 2). The embryo is elongated, and its long and short axes measure 658 and 560 μm, respectively. Fig. 1*A* displays an external view from the right side of the embryo along its long axis. There is a micromere cap at one end (right: A) and larger macromeres are at the opposite end (left: P). By homology with many modern embryos, these might be interpreted as anterior pole (right) and posterior pole (left) (16, 17). External views of the micromere cap and macromeres can also be seen in Fig. 2*A* and *B*. Fig. 1*B* shows a digital internal section cut halfway inward from the right surface (Fig. 1*A*) that represents a middle plane along the anterior-posterior axis. It shows dorso-ventral asymmetry, with large internal cells located at the putative posterior pole and in the ventral region, and smaller anterior cells. A second internal digital section is seen in Fig. 1*C*. Here the embryo has been rotated 30° along the same axis, top down away from the observer. This view is particularly interesting because it shows a series of flatter ectoderm-like cells extending around the periphery from about seven o'clock to about two o'clock, with a cell apparently missing at the top. These cells are closely applied to the underlying cells and to one another. A further 60° rotation on the same axis in the same direction arrives at the tangential plane and shows a subsymmetry of the specimen in the left-right direction (Fig. 1*D*). Figs. 1 and 2 show the distribution of flattened ectodermal cells on all but the ventral and ventral-lateral surfaces of the embryo. The cells on both the ventral (Fig. 1 *B* and *E*) and ventro-lateral surfaces (Fig. 2 *C*1, *C*2, *D*1, and *D*2) are subspherical, suggesting that the external cap did not extend ventrally to cover them. The views of the ventral surface shown in Fig. 1*E* and the sections shown in Fig. 1 *B* and 2 *C*1, *C*2, *D*1, and *D*2 reveal that the ectodermal layer did not extend across the ventral surface where large cells can be seen from the outside. However, the possibility that this configuration resulted from a secondary loss of ectodermal cells in this area cannot be ruled out. Subsymmetry in the bilateral direction of this embryo is suggested by the external view of the presump-

Author contributions: J.-Y.C., D.J.B., and M.G.H. designed research; J.-Y.C., G.L., F.G., A.R.C., C.-Y.Z., D.-C.X., X.L., and Z.-J.Y. performed research; G.L., F.G., and P.T. analyzed data; and J.-Y.C., D.J.B., and M.G.H. wrote the paper.

The authors declare no conflict of interest.

This article is a PNAS Direct Submission.

[1]To whom correspondence should be addressed. E-mail: chenjunyuan@163.net.

This article contains supporting information online at www.pnas.org/cgi/content/full/0904805106/DCSupplemental.

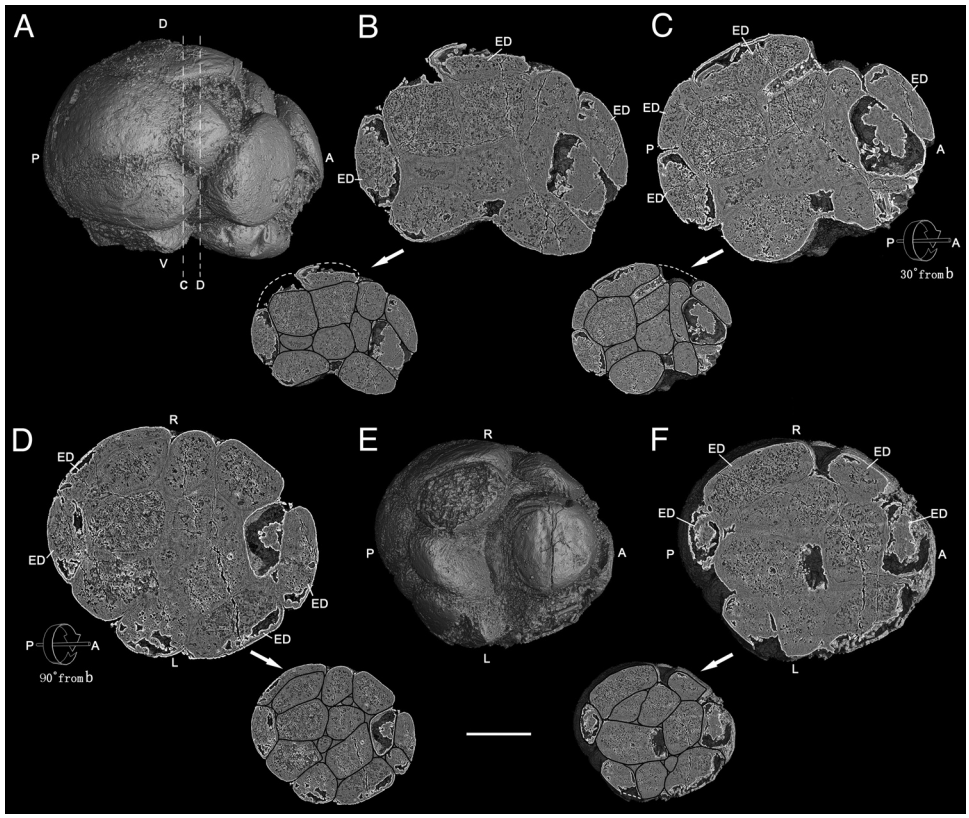

Fig. 1. Precambrian postgastrular embryo (4F10) from the Weng'an Phosphate Member of the Doushantou Formation showing external view from right side (*A*) and ventral side (*E*), and digital internal sections (*B, C, D*, and *F*) and the same sections (*B, C, D*, and *F*) with drawings of cell boundaries (in reduced size) along the a-p axis. (*A*) External view from right side along the anterior (right) and posterior (left) axis with lines C and D showing the locations of the internal digital sections seen in Fig. 2. (*B*) Digital internal section and the same section with drawing of cell boundaries at reduced size cut half way into the embryo from the right surface (Fig. 1*A*), showing maximal dorso-ventral asymmetry and ectodermal cells. (*C*) Digital internal section and the same section with drawing of cell boundaries at reduced size along the same (a–p) axis as Fig. 1*B* with 30° rotation top down away from the observer showing transition from asymmetry (Fig. 1*B*) to bilateral subsymmetry (Fig. 1*D*). (*D*) After 90° rotation from Fig. 1*B*, internal section and the same section with drawing of cell boundaries at reduced size showing the plane of left-right bilateral subsymmetry. (*E*) External digital view from the ventral side, revealing exposed, putative endodermal cells. (*F*) Internal section and the same section with drawing of cell boundaries at reduced size cut inward 23% from ventral surface (Fig. 1*E*), showing left-right, bilateral subsymmetry of the massive internal cells. (Scale bar, 250 μm.) Key: A, anterior; P, posterior; D, dorsal; V, ventral; R, right side; L, left side; ED, ectodermal cell.

tive ventral surface (Fig. 1*E*) and a computational section 23% inward from the ventral surface and parallel to it (Fig. 1*F*). The interior intercellular junctions of the external and internal cells of the embryo are thickened by diagenetic crusts, but this does not obscure the arrangement or internal structures of these cells, as demonstrated by the drawing of cell boundaries for internal sections (Figs. 1 and 2). Many of the cells, especially internal cells both in Figs. 1*D* and 5*A*, display prominent dark-colored cytoplasmic inclusions of 15–17 μm in size, being irregular or spherical. Because the image is based on electronic density, these dark-colored inclusions reflect relatively lower electronic density, which may indicate that they contain more organic matter.

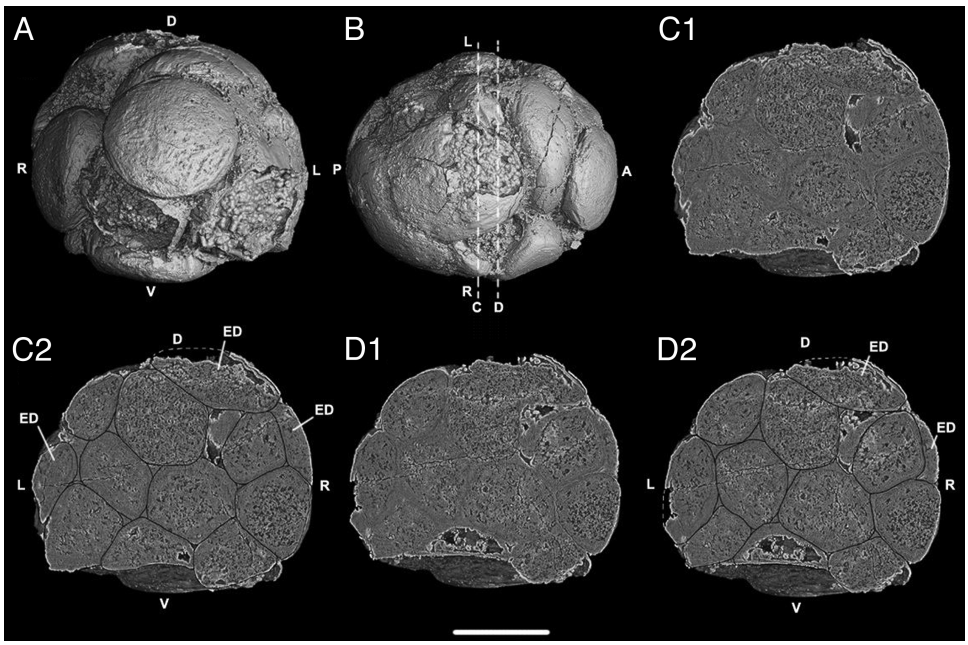

Fig. 2. Precambrian postgastrular embryo (4F10) from the Weng'an Phosphate Member of the Doushantou Formation showing external view from apical pole (*A*) and dorsal side (*B*) with two digital internal sections (*C*1, *D*1) and the same sections with drawings of cell boundaries (*C*2, *D*2), at locations indicated at lines C and D (Fig. 1*A*, Fig. 2*B*). (Scale bar, 250 μm.) Key: A, anterior; P, posterior; D, dorsal; V, ventral; R, right side; L, left side; ED, ectodermal cell.

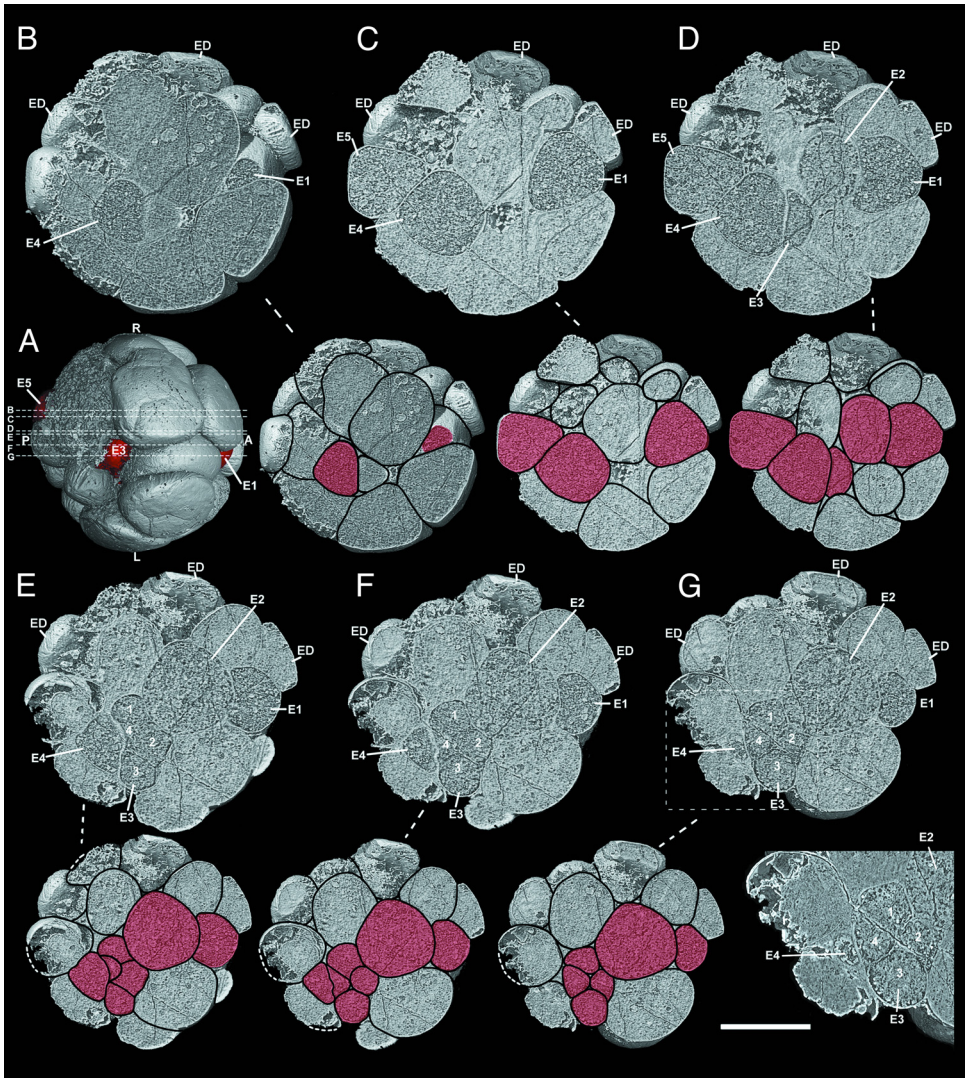

Fig. 3. Precambrian postgastrular embryo (4F4) from the Weng'an Phosphate Member of the Doushantou Formation as serial digital sections that cut in at successively deeper layers from the right surface, indicated by the lines B–G both in Fig. 3*A* and Fig. 4 *D* and *E*, and the same sections with drawings of cell boundaries. (*A*) Digital external view from ventral side of the embryo 4F4, showing: E5, E3, and E1 cells (in red) and the positions of digital internal sections in Fig. 3 *B*–*G* indicated by lines B–G. (*B*) Internal section and the same section with drawing of cell boundaries at reduced size cut in 29% from right surface, showing principal endodermal cells E4 and E1 sectioned near the right margin of the endodermal cord. (*C*) 35% from right surface, showing endodermal cells E5, E4, and E1. (*D*) 43% from right surface. (*E*) 46% from right surface. (*F*) 51% from right surface. (*G*) 53% from right surface, showing most parts of the endodermal cord, close to the middle plane of the embryo, and cluster of four cells, apparently the daughter cells resulting from mitosis of E3 (enlarged in lower right panel). Key: A, anterior; P, posterior; D, dorsal; V, ventral; L, left side; R, right side; and ED, ectodermal cell. In reduced sections with cell boundaries drawn endodermal cells are in red. (Scale bar: 250 μm in digital sections, 375 μm in the same section with drawing of cell boundaries, 181 μm in the lower right panel.)

We interpret these inclusions as the remains of yolk granules, similar to those that have been found in other Doushantuo embryos by (4, 11).

Another highly organized, spherical, multicellular embryo (4F4), about 750 μm in diameter, is illustrated in Figs. 3 and 4. Based on counts of cells present (25 cells) and clear evidence of broken cells on its surface, it is about a 32-celled embryo (Movie S2). The organization of this embryo reveals a number of bilaterian characters. As immediately evident in Fig. 3, this fossil embryo contains a distinct internal cell type. These cells are densely packed with inclusions, which are minute and preserved in darker color than the contents of other cells in the embryo. We interpret them as the remains of yolk granules (4, 11), similar but not identical to those seen in embryo 4F10 (Fig. 5*A*). Fig. 3 shows a series of digital internal sections (see Figs. 3*A* and 4 *D* and *E*) cut into the embryo from the right surface, revealing that the putative yolky cells form a cord-like structure consisting of four large cells (E1, E2, E4, and E5) plus a cluster of four small cells in the middle, apparently the daughter cells of cell E3 that underwent mitosis (Fig. 3 *E*–*G*). These cells form a contiguous, linearly aligned cord (Fig. 4 *C* and *F*). We interpret these yolk-rich internal cells as endodermal cells, and refer to this elongated cord of cells as the endodermal cord, with E1 at what might be the anterior end and E5 the posterior end. Analysis of the sections using the segmentation utility revealed that the cord is complex in shape, and digital isolation of individual endodermal cells shows that it is bent into a shallow S shape both laterally and ventro-dorsally. Fig. 4*A* is an external view of the embryo from the right side, the same orientation as the digital sections in Fig. 3, and it shows that the red-colored putative endodermal cord is exposed externally at its anterior and posterior ends (E3 is exposed to the outside because of a missing external cell; Figs. 3*A* and 4*D*). Fig. 4*B* is a transparent view from this same side, in which the cells of the putative endodermal cord are colored red. Fig. 4*C* shows the cord isolated from the rest of the embryo. An equivalent set of images from the dorsal side of the embryo is shown in Fig. 4 *D*–*F*. We see here that the putative endodermal cord deviates toward the right from the medial plane. Nonetheless, this cord-like structure could be comparable to the precursor of the anterior to posterior gut, a bilaterian character.

In addition to the endodermal cord cells in embryo 4F4 is a layer of smaller, flattened cells that forms what may be an ectodermal cap covering the dorsal and lateral surfaces of the embryo (Figs. 3 and 4). This cap is evident in all parts of Fig. 3. Cells on the ventral surface are larger and subspherical (Fig. 3 *C*–*G*), suggesting that the ectodermal layer did not yet extend far enough ventrally to cover them. Note that in this very well preserved specimen, 4F4, the cell boundaries are clear and sharp and do not display the diagenetic accretions seen in embryo 4F10 in Figs. 1 and 2.

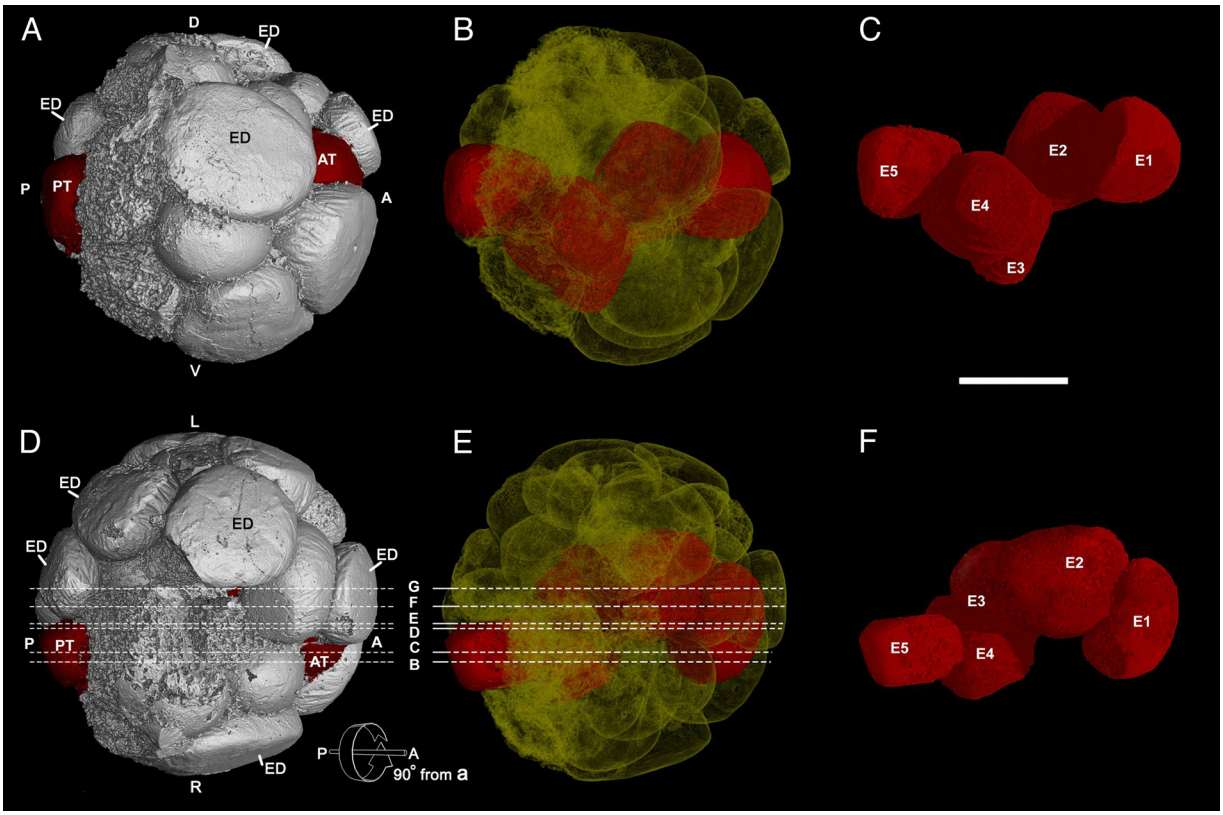

Fig. 4. Precambrian postgastrular embryo (4F4) from the Weng'an Phosphate Member of the Doushantou Formation. (*A*) Digital external view from right side along the anterior (right: A) and posterior (left: P) axis, showing: anterior (AT) and posterior (PT) terminations (in red) of the putative endodermal cord of cells, and presumed ectodermal cells on dorsal surface. (*B*) Transparent view from right side, showing the putative endodermal cord of cells (in red) that has a shallow S shape dorso-ventrally, and extends through the embryo from anterior to posterior ends. (*C*) Digital view of the putative endodermal cord seen laterally from the right side with its constituent cells coded as E1–E5. (*D*) Digital external view from dorsal side of the embryo, showing: the cells at the anterior (AT) and posterior (PT) terminations of the putative endodermal cord (in red); the lines designated B–G represent the locations of digital sections shown in Fig. 3 *B*–*G*. (*E*) Digital transparent view from dorsal surface, showing the putative endodermal cord (red), curved into a shallow S shape laterally; the lines B-G representing locations of the section shown in Fig. 3 *B*–*G*. (*F*) Digital view of the endodermal cord from dorsal side and its constituent cells coded as E1–E5. (Scale bar, 250 μm.) The endodermal cells were isolated and colored with the segmentation program of VG studio Max 1.21. Key: A, anterior; P, posterior; AT, anterior termination; PT, posterior termination; D, dorsal; V, ventral; L, left side; R, right side.

The preservation of cell nuclei has been reported in numerous fossil cells including possible examples from other Doushantuo embryos (4). A putative nucleus that is spherical, about 50 μm in diameter, and contains two small dark-colored inclusions is found within a cell of embryo 4F4, and one of these two inclusions, which are spherical and about 10 μm in diameter, may represent a possible nucleolus (Fig. 5 B and *C* and Movie S3).

Discussion

Although composed of a relatively small number of cells, both of the fossil embryos described here display complex, organized

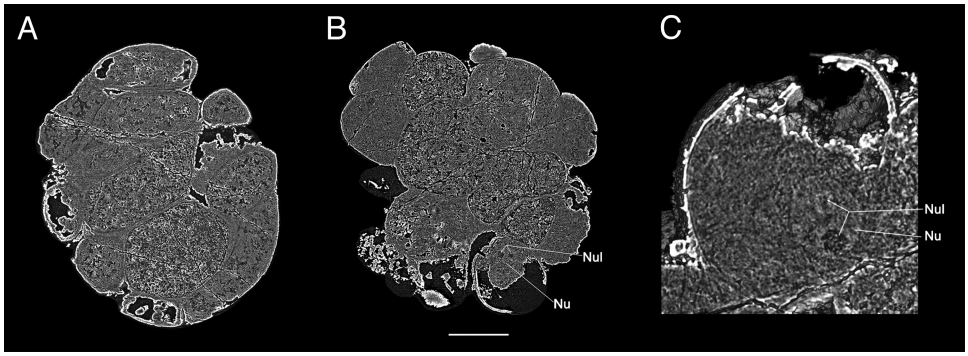

Fig. 5. Preservation of yolk granules and possible nucleus. (*A*) Internal section cut inward 39% from dorsal surface, showing detail of the yolk-rich, internal cells in embryo 4F10. (*B*) A digital thin slice (0.1-μm thick) of an internal section of embryo 4F4 46% from right surface (rotated, but same plane of section as in Fig. 3*E*), revealing the yolk-rich endodermal cells, as well as the location of a putative nucleus and nucleolus. (*C*) Internal section of Fig. 5*B* cell showing a close-up of the putative nucleus and nucleolus, as seen in Movie S3. Key: Nu, nucleus; Nul, nucleolus. (Scale bar, 142 μm in *A*, 156 μm in *B*, and 49 μm in *C*.)

patterns, and differentiated cell types seen in early gastrulae of some existing invertebrates. The symmetrical and structural characteristics of the embryos suggest they have anterior-posterior, dorsal-ventral, and right-left axes. The elongate embryo 4F10 (Figs. 1 and 5*A*) resembles a postgastrular bilaterian embryo, and embryo 4F4 (Figs. 3 and 4) is perhaps a stage still completing gastrulation. Cleaveage stages similar to these and resulting from large yolky eggs, which would be the case with both embryos, typically achieve internalization of the yolky endodermal cells by epiboly (16–18). During epibolic gastrulation, presumptive ectodermal cells at the animal pole of the embryo proliferate more rapidly than the yolk-rich endodermal cells, and move in a vegetal direction to cover the endoderm. The endodermal cells of 4F4 contain rich dark-colored inclusions (Figs. 3 and 5*B*), which are similar to those in 4F10 and interpreted as the remains of yolk granules. In gastrular stages of many living invertebrates, the ectodermal cells are smaller than the internalized endoderm and form a layer of thin, flattened cells overlying the internalized endoderm, a situation seen in both fossil embryos described here. Additionally, the absence of a blastocoel is not unusual in cleavage stages resulting from large yolky eggs. Such stages are observed in some turbellarian flatworms, polychaetes, and mollusks (16, 18).

The organization of presumptive ectoderm and endoderm in embryo 4F4 (Figs. 3 and 4) is not typical of any known animal of which we are aware. The disposition of the putative endodermal cord in unique in being exposed to the outside at both anterior and posterior ends. Although epibolic gastrulation of large yolky eggs in many animal embryos terminates at a vegetal position leaving some endoderm cells exposed (i.e., as a blastopore), no living animals leave two sites of endodermal exposure. However, we should not be surprised that the embryos of the earliest animals are not exactly like those seen after 600 million years of evolution.

Despite similarities in apparent mode of gastrulation, these two fossil embryos display clearly different spatial organizations of their cells. These major differences in internal patterning and in right-left symmetry suggest that rather than representing different stages in the developmental sequence of the same animal, these two embryos belong to two different animal taxa. This in itself shows that the stage of metazoan evolution represented by these Doushantuo specimens postdates the last common bilaterian ancestor. This conclusion is in accord with other fossil studies (6, 19–20), as well as conclusions drawn from molecular phylogeny, which places this ancestor in the late Cryogenian at 635 ma or greater and hence before the end of Snowball Earth (21–22).

Materials and Methods

The Doushantuo Formation has been intensively quarried for phosphates at the Wusi, Baishaikang, and Nanbao quarries along the axis of the Mt. Beidou anticline near Weng'an in Guizhou Province, southern China (9). The specimens for this study came from the gray facies of the Weng'an Phosphate Member exposed at these quarries. The specimens used for PPC- SR-μCT came from rock samples that were broken into pieces that were a few centimeters in greatest dimension and then were submerged in a 10% acetic acid solution.

About 100 specimens were selected from the acid residue for PPC- SR-μCT and imaged on the beamline ID19 at the European Synchrotron Radiation Facility. The detector was based on a CCD FreLoN camera linked to a revolver microscope optic. Depending on the sample sizes, we used isotropic voxel sizes of 0.28, 0.56, and 0.7 μm. The beam was monochromatized at an energy of 20.5 keV using a multilayer monochromator. To obtain a phase-contrast effect, we used a sample-detector distance (propagation distance) between 15 and 50 mm depending on the pixel size, and 1,500 projections on 180°. The software VGStudioMax 1.2 and 2.0 (Volume Graphics) were used for 3-D data processing, segmentation, and analysis.

ACKNOWLEDGMENTS. We thank Eric Davidson for aid and support throughout the analysis of these specimens and completion of this paper, Jon Mallatt and Stephen Q. Dornbos for helpful comments on the manuscript, and X.-Z. Li and Z.-Z. Mu for technical assistance. This work was supported by Chinese Academy of Science Grants KZCX3-SW-14 and 542006IHEPZZBS50639; National Basic Research Program of China Grants 2007CB815800 and 2006CB806400; National Science Foundation of China Grants 40432006, 40772001, and 10675140); European Synchrotron Radiation Facility (ID19 beamline) for beamtime access (proposal ec-138); 111 and 985–2 Projects of Nanjing University; Caltech through the Gordon and Betty Moore Distinguished Scholar Program (to J.-Y.C.); National Aeronautics and Space Administration Ames Research Center Grant NAG2–1541 and the University of Southern California (to D.J.B.); the Beckman Institute (to R.A.C.), and the Caltech Camilla Chandler Frost Fellowship (to F.G.).

1. Condon D, et al. (2005) U-Pb ages from the Neoproterozoic Doushantuo Formation, China. *Science* 308:95–98.
2. Chen DF, Dong WQ, Zhu BQ, Chen XP (2004) Pb-Pb ages of Neoproterozoic Doushantuo phosphorites in South China: Constraint on early metazoan evolution and glaciations events. *Precambrian Res* 132:123–132.
3. Barfod GH, et al. (2002) New Lu-Hf and Pb-Pb constraints on the earliest animal fossils. *Earth Planet Sci Lett* 201:203–212.
4. Hagadorn JW, et al. (2006) Cellular and subcellular structure of Neoproterozoic animal embryos. *Science* 314:291–294.
5. Xiao S, Zhang Z, Knoll AH (1998) Three dimensional preservation of algae and animal embryos in a Neoproterozoic phosphorite. *Nature* 391:553–558.
6. Chen J-Y, et al. (2006) Phosphatized polar lobe-forming embryos from the Precambrian of southwest China. *Science* 312:1644–1646.
7. Li C-W, Chen J-Y, Hua T-E (1998) Precambrian sponges with cellular structures. *Science* 279:879–882.
8. Bailey JV, Joye SB, Kalanetra KM, Flood BE, Corsetti FA (2007) Evidence of giant sulphur bacteria in Neoproterozoic phosphorites. *Nature* 445:198–201.
9. Chen J-Y (2004) *The Dawn of Animal World* (Publishing House of Jiangsu Science and Technology, Nanjing).
10. Xiao S, Knoll.AH (2000) Phosphatized animal embryos from the Neoproterozoic Doushantuo Formation at Weng'an, Guizhou, South China. *Jour Paleontology* 74:767–788.
11. Chen, J-Y, et al. (2009) Phase contrast synchrotron X-ray microtomography of Ediacaran (Doushantuo) metazoan microfossils: Phylogenetic diversity and evolutionary implications. *Precambrian Res* 173:191–200.
12. Tafforeau P, et al. (2006) Application of X-ray synchrotron microtomography for non-destructive 3D studies of paleontological specimens. *Applied Physics A* 83:195–202.
13. Friis EM, et al. (2007) Phase-contrast X-ray microtomography links Cretaceous seed with Gnetales and Bennecttitales. *Nature* 450:549–553.
14. Lak M, Néraudeau D, Nel A, Cloetens P, Perrichot V, Tafforeau P (2008) Phase contrast X-ray synchrotron imaging: Opening access to fossil inclusions in opaque amber. *Microsc Microanal* 14:251–259.
15. Donoghue PCJ, et al. (2006) Synchrotron X-ray tomographic microscopy of fossil embryos. *Nature* 442:680–683.
16. Kume M, Dan K (1968) *Invertebrate Embryology.* English translation by Jean C. Dan. (National Library of Medicine, Public Health Service, U.S. Dept. of Health, Education and Welfare and National Science Foundation, Washington, DC and NOLIT Publishing House, Belgrade).
17. Gilbert SF, Raunio AM, eds. (1997) Embryology, Constructing the Organism (Sinauer, Sunderland, MA), pp 1–537.
18. Raven CP (1966). Morphogenesis: The Analysis of Molluscan Development, 2nd ed. (Pergamon, Oxford), pp 1–365.
19. Chen J-Y, et al. (2000) Precambrian animal diversity: Putative phosphatized embryos from the Doushantuo Formation of China. *Proc Natl Acad Sci* USA 97: 4457.
20. Chen J-Y, et al. (2004) Small bilaterian fossils from 40 to 55 million years before the Cambrian. *Science* 305:218–222.
21. Douzery EJP, Snell EA, Bapteste E, Delsuc F, Philippe H (2004) The timing of eukaryotic evolution: Does a relaxed molecular clock reconcile proteins and fossils. *Proc Natl Acad Sci USA* 101:15386–15391.
22. Peterson KJ, Cotton JA, Gehling JG, Pisani D (2008) The Ediacaran emergence of bilaterians: Congruence between the genetic and the geological fossil records. *Phil Trans R Soc B* 363:1435–1443.